On the numerical solution of a driven thin film equation

Youngsoo Ha [a], Yong-Jung Kim [a,*], Tim G. Myers [b]

[a] *Department of Mathematical Sciences, KAIST (Korean Advanced Institute of Science and Technology),*
335 Gwahangno Yuseong-gu, Daejeon 305-701, Republic of Korea
[b] *Department of Mathematics & Applied Mathematics, University of Cape Town, South Africa*

Abstract

This paper is devoted to comparing numerical schemes for a differential equation with convection and fourth-order diffusion. Our model equation is $u_t + (u^2 - u^3)_x = -(u^3 u_{xxx})_x$, which arises in the context of thin film flow. First we employ implicit schemes and treat both convection and diffusion terms implicitly. Then the convection terms are treated with well-known explicit schemes, namely Godunov, WENO and an upwind-type scheme, while the diffusion term is still treated implicitly. The diffusion and convection schemes are combined using a fractional step-splitting method.
© 2008 Elsevier Inc. All rights reserved.

1. Introduction

In this paper we consider numerical solutions to the following equation

$$u_t + f(u)_x = -(u^3 u_{xxx})_x, \tag{1.1}$$

where the flux is given by

$$f(u) = u^2 - u^3. \tag{1.2}$$

Eq. (1.1) describes the flow of a thin liquid film, where $u(x,t) \geqslant 0$ denotes the film thickness. The flux terms represent surface shear and gravity, where the forces act in opposing directions, the diffusion term on the right hand side represents surface tension. The surface shear term may arise due to temperature or concentration gradients or to an external shear force (caused by wind for example). Derivations of Eq. (1.1) and related equations may be found in the reviews [21,25]. For the specific case when thermocapillary effects produce the surface shear, Eq. (1.1) is derived in [4,11], with a wind induced stress a derivation is given in [22,23]. Experimental results showing typical film shapes for thermocapillary flow up a vertical plate are presented in [11]. The experiments show good agreement with numerical solutions for the small times that the

---

* Corresponding author. Tel.: +82 42 869 2739; fax: +82 42 869 5710.
E-mail addresses: young@amath.kaist.ac.kr (Y. Ha), yongkim@kaist.edu (Y.-J. Kim), timothy.myers@uct.ac.za (T.G. Myers).

experiments have been run [3]. However, it is the properties of the numerical solution that we are focussing on, not the comparison with experiment.

The numerical solution of Eqs. (1.1) and (1.2) is constrained by the diffusion term. An explicit scheme requires a time-step Δt of the order $(\Delta x)^4$. Consequently in regions where high resolution is required, such as at a moving front, a singularity or at blow-up, the computational time is prohibitive. Implicit methods are therefore generally preferred. Recently these have been coupled with adaptive meshes to permit high accuracy in the regions of primary interest, see [2,12,27,33] for example. However, the first-order convection term is not subject to the same constraint and there are many different methods to deal with nonlinear convection. In the following work we focus primarily on a comparison between finite difference, Godunov, an adapted upwind and WENO schemes applied to the convection term. We also investigate the effect of applying fully implicit and Crank–Nicolson schemes. Even if it is possible to solve the full equation in a single step with implicit schemes, fractional step splitting, alternating between solving for the diffusion and convection terms, is applied in all cases for consistency in the tests.

The majority of our numerical examples will be taken from [4]. We use these examples because Bertozzi et al. [4] present a very careful numerical and analytical investigation of Eqs. (1.1) and (1.2) and the cases presented show a wide variety of behaviour in the solutions. The flux function has a point of inflexion at $u = 1/3$. The form of solution is likely to change around this point, consequently in our numerical solutions we will take limiting values for u close to this value.

2. Numerical schemes

The notation employed in the numerical calculations is as follows. We consider a uniform mesh $x_{j+1/2}$ with a fixed width $h \equiv \Delta x > 0$, where $x_{j+1/2} = (j + 1/2)h$, $j \in \mathbf{Z}$. The time mesh is given by $t^n = n\Delta t$, with a fixed time step size $\Delta t > 0$. A solution to a nonlinear convection equation may have a discontinuity and its numerical correspondence U_j^n is usually considered as the approximation to the cell average of the true solution, i.e.,

$$U_j^n \cong \frac{1}{h} \int_{x_{j-1/2}}^{x_{j+1/2}} u(x, t^n)\mathrm{d}x. \tag{2.1}$$

We use a fractional step-splitting method to handle two terms in Eq. (1.1). The convection term will be tackled via various implicit and explicit finite difference (or finite volume) methods which will be given in the following section. We will observe the performance differences made by these schemes for the convection part. The diffusion term will always be dealt with via an implicit method.

2.1. Finite difference for the diffusion term

First consider a finite difference scheme for the diffusion equation

$$u_t = -\phi(u)_x, \quad \phi(u) = u^3 u_{xxx}. \tag{2.2}$$

We view $u_{j+1/2}^n$ as a time average of $u(x, t)$ on the interval $t \in [t^n, t^{n+1}]$ at the interface $x = x_{j+1/2}$. Then, after integrating (2.2) over the mesh $[x_{j-1/2}, x_{j+1/2}] \times [t^n, t^{n+1}]$, one can easily check that the cell averages given by (2.1) satisfy

$$U_j^{n+1} = U_j^n - \frac{\Delta t}{h}(\phi(u_{j+1/2}^n) - \phi(u_{j-1/2}^n)), \tag{2.3}$$

where we view $\phi(u_{j+1/2}^n)$ as a time average of the diffusive flux on the interval $t \in [t^n, t^{n+1}]$ at the interface $x = x_{j+1/2}$. Since

$$u(x + 2h) - 3u(x + h) + 3u(x) - u(x - h) = h^3 u_{xxx}(x + h/2) + \mathrm{O}(h^5),$$

we obtain the following finite difference representation

$$h^3\phi(u_{j+1/2}^n) \cong \left(\frac{U_{j+1}^n + U_j^n}{2}\right)^3 (U_{j+2}^n - 3U_{j+1}^n + 3U_j^n - U_{j-1}^n) =: \Phi_{j+1/2}(U^n).$$

However, this approximation is impractical since the time step Δt should be of order h^4 to be stable which demands a huge computation time. Therefore, we consider an implicit method given by

$$U_j^{n+1} = U_j^n - \frac{\Delta t}{h^4}[\theta(\Phi_{j+1/2} - \Phi_{j-1/2})(U^n) + (1-\theta)(\Phi_{j+1/2} - \Phi_{j-1/2})(U^{n+1})], \tag{2.4}$$

where θ is a weighting factor. If $\theta = 0.5$, then the method is Crank–Nicolson, with second order accuracy in space and time. If $\theta = 0$, then the method is fully implicit, with first order in time and second order in space. If $\theta = 1$, then it gives an explicit method.

We are interested in the behaviour of a solution on the whole real line. However, since the domain of computation should be finite, a numerical boundary condition is required. Since the solution is expected to be flat for $|x|$ large, we take boundary conditions,

$$u_x(a,t) = u_x(b,t) = 0, \quad t > 0,$$

where the interval $[a,b]$ is the domain of the computation. To impose these boundary conditions numerically we simply add two more imaginary boundary points and assign them the value at the boundary.

2.2. Finite difference for the convection term

We now consider a numerical scheme for the convection part,

$$u_t = -f(u)_x. \tag{2.5}$$

Integrating (2.5) over the mesh $[x_{j-1/2}, x_{j+1/2}] \times [t^n, t^{n+1}]$ similarly shows that the cell averages satisfy

$$U_j^{n+1} = U_j^n - \frac{\Delta t}{h}(f(u_{j+1/2}^n) - f(u_{j-1/2}^n)). \tag{2.6}$$

A numerical scheme given in this form is called a conservative one and gives correct speeds of possibly discontinuous waves. The choice of numerical scheme determines the *intercell (time) average flux*,

$$f(u_{j+1/2}^n) \cong f(u(x_{j+1/2}, t)), \quad t^n \leqslant t \leqslant t^{n+1}. \tag{2.7}$$

In a numerical scheme the average flux $f(u_{j+1/2}^n)$ or the average itself, $u_{j+1/2}^n$, is approximated using its neighboring cell averages. For explicit schemes the cell averages at the time step n are used

$$f(u_{j+1/2}^n) \cong F(U_{j-k_1}^n, \ldots, U_{j+k_2}^n) =: F_{j+1/2}(U^n).$$

In this notation $F_{j+1/2}(U^n)$ should be understood as the intercell average flux at the interface $x_{j+1/2}$ obtained using sequence U^n. Then, implicit methods are obtained by replacing U^n with U^{n+1}, i.e.,

$$f(u_{j+1/2}^n) \cong F(U_{j-k_1}^{n+1}, \ldots, U_{j+k_2}^{n+1}) = F_{j+1/2}(U^{n+1}).$$

Many schemes have been developed and are widely used to deal with convection. We will now investigate the application of Godunov, an adapted upwind and WENO methods to the convection equation (2.5).

2.2.1. Crank–Nicolson and a fully implicit scheme

The Crank–Nicolson scheme is obtained by approximating the intercell time average by the flux average using four adjacent cells, i.e.,

$$f(u_{j+1/2}^n) \cong \frac{1}{4}(f(U_j^n) + f(U_{j+1}^n) + f(U_j^{n+1}) + f(U_{j+1}^{n+1})).$$

Then the corresponding numerical scheme is written as

$$U_j^{n+1} = U_j^n - \frac{\Delta t}{4h}[(f(U_{j+1}^{n+1}) - f(U_{j-1}^{n+1})) + (f(U_{j+1}^n) - f(U_{j-1}^n))]. \tag{2.8}$$

This Crank–Nicolson scheme is partly implicit. If an approximation $f(u_{j+1/2}^n) \cong \frac{1}{2}(f(U_j^{n+1}) + f(U_{j+1}^{n+1}))$ is taken, then one obtains

$$U_j^{n+1} = U_j^n - \frac{\Delta t}{2h}(f(U_{j+1}^{n+1}) - f(U_{j-1}^{n+1})), \tag{2.9}$$

which will be called a fully implicit method in this paper. The diffusion term in (1.1) should be tackled via an implicit method since it takes too much computational time to treat a fourth-order term explicitly. Therefore, these implicit methods have the advantage of simplicity, in that all terms in the full governing equation can be dealt with in the same manner.

2.2.2. Godunov scheme

Godunov schemes [6,18,19,31] are based on the solution of the Riemann problem using characteristic information within the framework of a conservative method. Since the flux is non-convex, one should consider convex–concave envelopes to construct Riemann solutions (see [14,15] for general non-convex fluxes).

Suppose that $u_l > u_r$ and the initial value is given by

$$u_0(x) = \begin{cases} u_l, & x < 0, \\ u_r, & x > 0. \end{cases}$$

Then the 'concave' envelope, say $k(u)$, of the flux in the domain $[u_r, u_l]$ should be considered, which is

$$k(u) := \inf_{\eta \in B} \eta(u), \quad B := \{\eta \in C^2(\mathbf{R}) : \eta''(u) \leqslant 0, \eta(u) \geqslant f(u) \text{ for } u_r < u < u_l\}.$$

The solution of the Riemann problem is

$$u(x, t) = \begin{cases} u_l, & x < a(t), \\ g(x/t), & a(t) < x < b(t), \\ u_r, & b(t) < x, \end{cases} \tag{2.10}$$

where the rarefaction profile $g(x)$ is given by the relation $k'(g(x)) = x$ and $a(t) = k'(u_l)t \leqslant k'(u_r)t = b(t)$. Similarly, if $u_l < u_r$, the rarefaction profile $g(x)$ is obtained after replacing the concave envelope with the 'convex' one,

$$l(u) := \sup_{\eta \in A} \eta(u), \quad A := \{\eta \in C^2(\mathbf{R}) : \eta''(u) \geqslant 0, \eta(u) \leqslant f(u) \text{ for } u_l < u < u_r\},$$

and $a(t) = l'(u_l)t \leqslant l'(u_r)t = b(t)$. Considering the structure of the flux $f(u) = u^2 - u^3$, one can easily see that

$$k'(g) = 0 \Longleftrightarrow g = 2/3 \quad \text{and} \quad l'(g) = 0 \Longleftrightarrow g = 0.$$

Therefore, the intercell time average $u_{j+1/2}^n$ may have values $u_l, u_r, 2/3$ or 0. If $0 \leqslant u(x, t) \leqslant \frac{2}{3}$, which is our domain of interest, then the envelopes are increasing functions in the domain and hence $a(t) \geqslant 0$ and $u_{j+1/2}^n = u_l$. In other words, the Godunov scheme is basically an upwind scheme, i.e.,

$$U_j^{n+1} = U_j^n - \frac{\Delta t}{h}(f(U_j^n) - f(U_{j-1}^n)). \tag{2.11}$$

The Godunov method can be modified to a second order scheme by employing a proper limiter. For this example we simply take

$$f(u_{j+1/2}^n) \cong f(U_j^n) + \frac{h}{2} f'(U_j^n) \left(1 - f'(U_j^n) \frac{\Delta t}{h}\right) \sigma_j^n,$$

where σ_j^n is a limiter. We use monotonized centered, van Leer (VL) or Superbee (SB) limiters in later examples (see [32] for example).

2.2.3. An adapted upwind scheme

An adapted Godunov-type semi-discrete scheme was introduced in [16,17] which gives the flexibility of central type schemes. We first compute the local speeds of propagation at the interface $x = x_{j+1/2}$. Since the speed of propagation is related to the CFL condition, we can estimate the local speeds of the right and left sides of the cell boundary. The local speeds of wave propagation are bounded by $s_{j+1/2,r}^n$ and $s_{j+1/2,l}^n$ which are given by

$$s_{j+1/2,r}^n = \max_C (f'(u), 0), \quad s_{j+1/2,l}^n = \min_C (f'(u), 0), \tag{2.12}$$

where $C = \{u : u \text{ is between } U_j^n \text{ and } U_{j+1}^n\}$. Employing these local speeds of propagation the intercell average flux is approximated by

$$f(u_{j+1/2}^n) \cong \frac{s_{j+1/2,r}f(u_{j+1/2}^-) - s_{j+1/2,l}f(u_{j+1/2}^+)}{s_{j+1/2,r} - s_{j+1/2,l}} + \frac{s_{j+1/2,r}s_{j+1/2,l}}{s_{j+1/2,r} - s_{j+1/2,l}}[u_{j+1/2}^+ - u_{j+1/2}^-], \tag{2.13}$$

where $u_{j+1/2}^+$ and $u_{j+1/2}^-$ are computed as

$$u_{j+1/2}^+ \equiv U_{j+1}^n - \frac{h}{2}(u_x)_{j+1}^n, \quad u_{j+1/2}^- \equiv U_j^n + \frac{h}{2}(u_x)_j^n,$$

$$(u_x)_j^n = \text{minmod}\left(\alpha \frac{U_{j+1}^n - U_j^n}{h}, \frac{U_{j+1}^n - U_{j-1}^n}{2h}, \alpha \frac{U_j^n - U_{j-1}^n}{h}\right), \quad 1 \leqslant \alpha \leqslant 2.$$

(Here, the 'minmod' function returns the input with the smallest absolute value if inputs are positively or negatively signed. Otherwise, it returns zero.) The effect of changing α is discussed in subsequent sections. In general we should take $\alpha \in [1, 2]$.

To obtain a better convergence order we take the three step TVD Runge–Kutta time discretization (see [28]),

$$U_j^{(1)} = U_j^n + \Delta t^n \mathcal{L}(U^{(0)}) \quad \text{with } U^{(0)} = U^n,$$

$$U_j^{(2)} = \frac{3}{4}U_j^n + \frac{1}{4}U_j^{(1)} + \frac{1}{4}\Delta t^n \mathcal{L}(U^{(1)}), \tag{2.14}$$

$$U_j^{n+1} = e^{\Delta t^n}\left(\frac{1}{3}U_j^n + \frac{2}{3}U_j^{(2)} + \frac{2}{3}\Delta t^n \mathcal{L}(U^{(2)})\right),$$

where $\mathcal{L}_j(U^{(k)}) = (F_{j+1/2}(U^{(k)}) - F_{j-1/2}(U^{(k)}))/h$. This semi-discrete scheme is of third order and also used for the WENO method in the following section. In the following we call this adapted Godunov-type semi-discrete scheme an adapted upwind (or simply an upwind) scheme.

2.2.4. WENO method

The weighted essentially non-oscillatory (or WENO) method is described in [7,8,10,20,28–30]. The ENO method has been combined with an adaptive mesh code in a study of the stability of moving contact lines in [12]. Greer et al. [5] compare a fifth order WENO and upwind schemes in a study of fourth-order partial differential equations on an arbitrary surface. They conclude that the requirements of accuracy and efficiency suggest that WENO is preferable to the other schemes.

We take the fifth order WENO method which has fifth (spatial) order accuracy in smooth regions and first order near a singularity. For the time discretization we use the third order semi-discrete scheme (2.14). To avoid entropy violating solutions and obtain numerical stability we split the flux $f(u)$ into two components f^+ and f^- such that

$$f(u) = f^+(u) + f^-(u), \tag{2.15}$$

where $D_u f^+ \geqslant 0$ and $D_u f^- \leqslant 0$. We take a Rusanov-type flux [26]

$$f^{\pm}(u) = \frac{1}{2}(f(u) \pm \gamma u), \tag{2.16}$$

where $\gamma = \max_u |f'(u)|$ over the pertinent range of u which can be decided *a priori*. Then the intercell average flux approximation is written as

$$f(u_{j+1/2}^n) \cong \frac{1}{12}(-f_{j-1} + 7f_j + 7f_{j+1} - f_{j+2}) - \Psi_N\left(\Delta f_{j-\frac{3}{2}}^+, \Delta f_{j-\frac{1}{2}}^+, \Delta f_{j+\frac{1}{2}}^+, \Delta f_{j+\frac{3}{2}}^+\right)$$

$$+ \Psi_N\left(\Delta f_{j+\frac{5}{2}}^-, \Delta f_{j+\frac{3}{2}}^-, \Delta f_{j+\frac{1}{2}}^-, \Delta f_{j-\frac{1}{2}}^-\right),$$

where $f_j = f(U_j^n)$, $f_j^{\pm} = f^{\pm}(U_j^n)$, $\Delta f_{i+\frac{1}{2}}^{\pm} = f_{i+1}^{\pm} - f_i^{\pm}$ and

$$\Psi_N(a, b, c, d) = \frac{1}{3}\omega_0(a - 2b + c) + \frac{1}{6}\left(\omega_2 - \frac{1}{2}\right)(b - 2c + d). \tag{2.17}$$

The nonlinear weights ω_0 and ω_2 are defined by

$$\omega_j = \frac{\gamma_j}{\sum_{l=0}^{k-1}\gamma_l}, \quad \gamma_l = \frac{d_l}{(\varepsilon + \beta_l)^2}, \quad d_0 = \frac{1}{10}, \quad d_1 = \frac{3}{5}, \quad d_2 = \frac{3}{10},$$

where, in this case, $k = 3$ and $0 < \varepsilon \ll 1$ is introduced to prevent singularity and the smoothness indicators β_j's are given by

$$\beta_0 = \frac{13}{12}(f_{i-2} - 2f_{i-1} + f_i)^2 + \frac{1}{4}(f_{i-2} - 4f_{i-1} + 3f_i)^2$$
$$\beta_1 = \frac{13}{12}(f_{i-1} - 2f_i + f_{i+1})^2 + \frac{1}{4}(f_{i-1} - f_{i+1})^2 \tag{2.18}$$
$$\beta_2 = \frac{13}{12}(f_i - 2f_{i+1} + f_{i+2})^2 + \frac{1}{4}(3f_i - 4f_{i+1} + f_{i+2})^2.$$

3. Computation of the convection and the diffusion

3.1. Linear transport equation

In this section we show two numerical examples for convection equations that highlight certain properties of interest to our subsequent calculations on the full problem.

Consider the linear transport equation

$$u_t + u_x = 0, \quad u(x,0) = u_0(x). \tag{3.1}$$

The exact solution of this problem is simply $u(x,t) = u_0(x - t)$. When we take sufficiently smooth initial data the numerical solutions for all the schemes introduced in Section 2, both implicit and explicit, provide accurate results. However, this is not the case with discontinuous data.

Consider the discontinuous initial profile

$$u_0(x) = \begin{cases} 2/3, & 0 < x < 1, \\ 0, & \text{otherwise.} \end{cases} \tag{3.2}$$

Numerical solutions using Crank–Nicolson, fully implicit and the Godunov method are shown as the solid lines on Fig. 1, with $h = 0.01$ and CFL numbers 0.025, 0.025, 0.75 for the respective schemes. The initial condition is shown as a dashed line. Only the Godunov scheme is shown, since other explicit schemes show indistinguishable results. Both implicit schemes show strong oscillations behind the discontinuity, although Crank–Nicolson is clearly the worst.

In general the oscillatory behaviour exhibited by Crank–Nicolson and fully implicit schemes forces the use of smooth initial data for the thin film equation (1.1). Godunov (and WENO and upwind) is designed to deal with convection equations with a possible discontinuity and consequently the solutions show no oscillations. In the numerical results of Section 4, where we incorporate the diffusion term, we will deal with both continuous and discontinuous initial data.

3.2. Convection with non-convex flux, $f(u) = u^2 - u^3$

Consider the conservation law, Eq. (1.1), with the diffusion term neglected

$$u_t + f(u)_x = 0, \quad f(u) = u^2 - u^3, \quad u(x,0) = u_0(x), \tag{3.3}$$

where the initial value is given by the discontinuous data of Eq. (3.2). This type of travelling wave is similar to the double shocks discussed in the following section. One can easily find the exact solution of the problem using rarefaction waves and the equal area rule [13]. This is shown as the dashed line in Fig. 2. Numerical solutions are also shown in the figures using the three explicit methods (the implicit methods all show severe oscillations and so are neglected). Away from the discontinuity all of the numerical solutions show excellent agreement with the exact solution. However, at the downstream side of the shock the solutions diverge, with
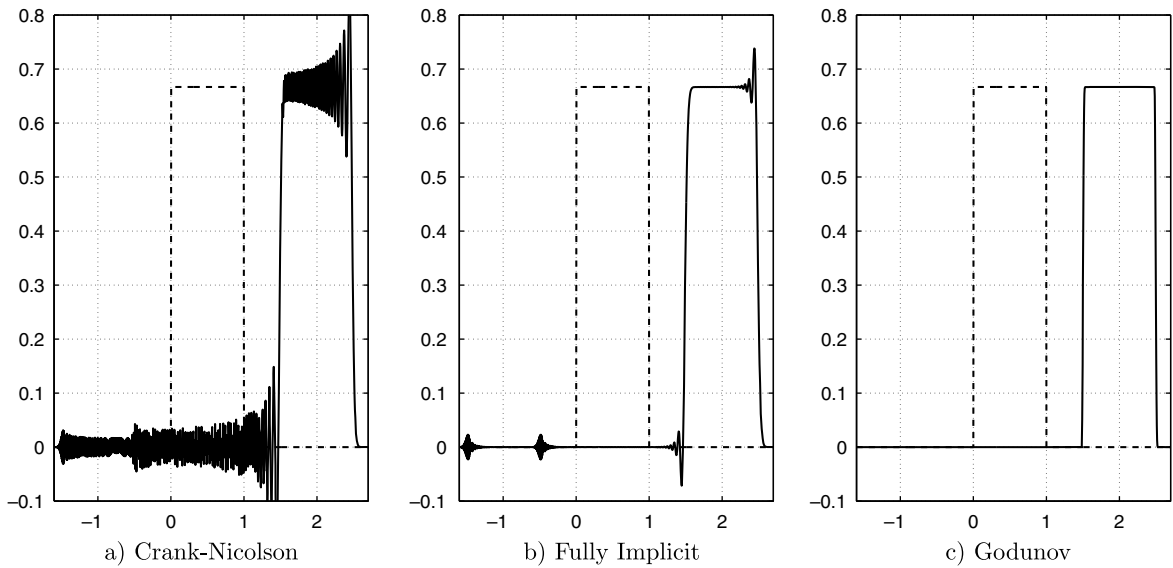
Fig. 1. Numerical solutions for the linear transport equation (3.1) with an initial value (3.2) shown as a dashed line. Here the mesh size is $h = 0.01$ and the CFL numbers are (a) 0.025, (b) 0.025 and (c) 0.75. The final computation time is $t = 1.5$.
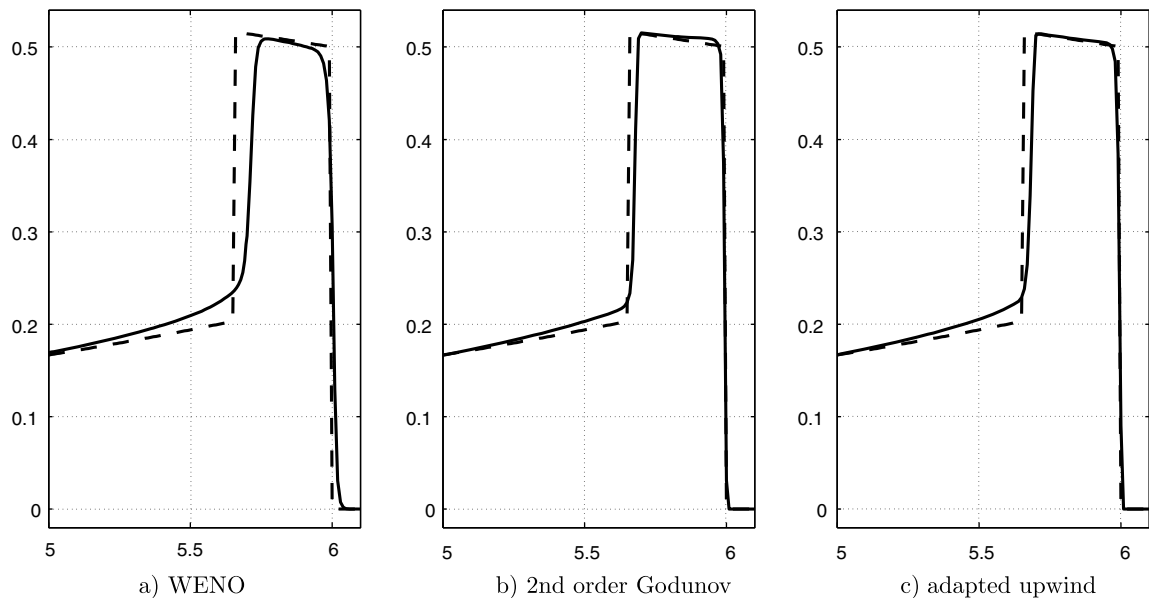

Fig. 2. Numerical solutions for the non-convex conservation law (3.3) with an initial value (3.2). Here the mesh size is $h = 0.01$ and the CFL numbers are (a) 0.5, (b) 0.75 and (c) 0.75, and the final computation time is $t = 20$. The exact solution is the dashed line.

WENO showing the greatest error. The second order Godunov shows a slightly lower error than the adapted upwind. On the upstream side all solutions show relatively good agreement.

The CFL number is the ratio of the physical wave speed over the numerical wave speed given by $\max_u f'(u)\Delta t/\Delta x$ and should be less than one for explicit schemes. Since the examples in this paper are all bounded by $0 \leqslant u \leqslant 2/3$, the maximum wave speed is $f'(1/3) = 1/3$. Therefore, the relation between time step size Δt is easily computed from the CFL number,

$$\Delta t = 3h \times \text{CFL}.$$

In the following examples we mostly give CFL numbers since it gives an extra physical meaning. The aim in choosing a CFL number is to accurately capture a discontinuity, without producing oscillations, while achieving a fast runtime. For a convex flux a high CFL, close to unity, is generally chosen for Godunov and upwind schemes. WENO usually requires a CFL around 0.5. In this paper, we deal with a non-convex flux. Taking a CFL of 0.9 in the above example for Godunov results in oscillations. We found a CFL of 0.75 removed the oscillations while retaining a fast runtime. A similar value was satisfactory for the upwind scheme, while WENO ran with good accuracy at the standard value of 0.5.

The results so far demonstrate the difficulty encountered by the implicit methods in the presence of a discontinuity. For small time-steps the fully implicit scheme shows relatively small oscillations, but large time-steps cause the solution to blow-up. Crank–Nicolson tends to show significant oscillations for a large range of time-steps but did provide a solution for all the cases investigated. The three explicit methods all deal well with discontinuities, with WENO showing slightly worse agreement with the exact solution than the other two. However, to obtain satisfactory solutions the CFL number should be around 0.75 for the upwind and Godunov and 0.5 for WENO.

3.3. Fourth-order diffusion $\phi(u)_x = (u^3 u_{xxx})_x$

It is clear that any second order polynomial in x is a steady state of Eq. (1.1) without the convection term, i.e.,

$$u_t = -\phi(u)_x, \quad \phi(u) = u^3 u_{xxx}. \tag{3.4}$$

Hence, $u(x, t) = x^2$ is an exact solution of the problem with the following initial and boundary condition

$$u(x, 0) = x^2 \quad \text{for } |x| < 1 \quad \text{and} \quad u(x, t) = x^2 \quad \text{for } |x| \geqslant 1, \ t \geqslant 0. \tag{3.5}$$

In Table 1 the error of the Crank–Nicolson method (2.4) for the diffusion equation is shown. Since the exact solution has zero value at the origin, the error at the origin is simply the value of the numerical approximation at that point. The test was performed under the two CFL numbers, 0.5 and 0.75, which were used in most of the numerical examples in this paper. We took 10^{-13} as the tolerance of the iteration procedure and the errors are less than this tolerance. This test indicates that the error for the diffusion term is small enough to be neglected in comparison with that of the full equation.

4. Computation of the full equation

Now we return to the original problem, specified by Eqs. (1.1) and (1.2), and compare the different numerical schemes. To solve the equation numerically we employ a fractional step splitting method that alternates between solving the diffusion equation (2.2) and the convection equation (2.5). In our tests step splitting with explicit convection schemes increased the stability of the solutions to such an extent that in the following examples we will not show any solutions obtained without step-splitting. In all of the following examples when we employ an explicit scheme to the convection term, we calculate the diffusion term using the Crank–Nicolson scheme. As will be seen later this is the most reliable of the two implicit schemes. From now on we will

Table 1
Errors of numerical solutions to (3.4) and (3.5) at the origin $x = 0$ are given, where the final computation time is $t = 1000$

# of mesh points	CFL=0.75	CFL=0.5
10	−4.5538e−16	2.2002e−16
20	−1.9401e−16	−1.4743e−16
40	6.1874e−17	4.2880e−16
80	1.0622e−16	1.1770e−16
160	−1.5062e−17	−2.9763e−17
320	1.2536e−17	−3.6033e−17
640	−1.2375e−17	−1.6552e−17

The numerical error of the diffusion equation is negligible in comparison to that of the full equation in Table 2.

refer to the schemes that involve explicit methods as the explicit schemes, despite the implicit diffusion component. This is to provide a simple distinction from the Crank–Nicolson and implicit schemes.

To clearly distinguish between the different schemes and avoid differences caused by the behaviour due to the initial condition it is best to compare results at large times. Obviously this can lead to large computational domains and consequently large computation times. In most examples we therefore modify equation (1.1) to move with the region of interest

$$u_t + f(u)_x - su_x = -(u^3 u_{xxx})_x, \tag{4.1}$$

where the wave speed s is the shock speed given by the Rankine–Hugoniot condition using the two boundary values,

$$s = \frac{f(u_r) - f(u_l)}{u_r - u_l}. \tag{4.2}$$

The addition of the new term means that we must introduce one more step to the splitting method

$$u_t = su_x. \tag{4.3}$$

To ensure that this part of the equation does not interfere with our investigation of the numerical schemes we compute (4.3) using a central method [9,24] for all cases.

4.1. Comparison of schemes for a travelling wave

Our aim in this section is to test the numerical schemes described in Section 2. We will do this by examining a standard thin film flow example of a travelling wave with a Lax shock. The travelling wave joins two regions of different heights, u_l and u_r, where

$$u_l = \lim_{x \to -\infty} u(x), \quad u_r = \lim_{x \to \infty} u(x).$$

In the limit $u_r \ll 1$ this can represent a thin film moving over a precursor layer. However, as pointed out in [4], any value of $0 < u_r < 1/3$ will show the same qualitative behaviour. Bertozzi et al. [4] show that multiple Lax shocks are possible for this situation, depending on the initial conditions. As discussed earlier, both Crank–Nicolson and fully implicit methods have difficulties in dealing with discontinuous initial values, hence they use a continuous initial condition involving a hyperbolic tangent. We will discuss the effect of discontinuous initial conditions in the following sections.

For comparison purposes we must first determine the travelling wave solution which obviously should propagate with no time variation. This solution will be imposed as the initial value for the numerical schemes. We may then test the accuracy of the schemes by observing how the numerical solutions diverge from the travelling wave over time. An alternative test would be to start with a smooth function, such as the hyperbolic tangent, and observe how the numerical solution tends to the travelling wave over time. However, our method allows us to make a meaningful comparison after a relatively short time and removes the problem of determining whether the error occurs because the numerical solution has not yet reached a steady state.

To determine the travelling wave solution we start by making the substitution $\xi = x - st$ where s is the wave speed. This allows Eq. (1.1) to be integrated once and written as

$$u_{\xi\xi\xi} = \frac{su + u^3 - u^2 + c}{u^3}. \tag{4.4}$$

The far-field solutions $x \to -\infty, u \to u_l$ and $x \to \infty, u \to u_r$ allow the values of s and c to be calculated

$$s = \frac{(u_l^2 - u_l^3) - (u_r^2 - u_r^3)}{u_l - u_r} = \frac{f(u_l) - f(u_r)}{u_l - u_r}, \quad c = u_l u_r (u_l + u_r - 1).$$

The wave speed is identical to that given by the Rankine–Hugoniot condition (4.2). The numerical solution of (4.4) is obtained by imposing the asymptotic solutions at either side and breaking the translational invariance, see [1] for example. In this case we match the x co-ordinate for the position of the maximum film height. Of

course since there may be some variation in this position with different schemes, particularly for large h, we cannot do this exactly and must therefore choose a best fit.

In the following calculations we will assume that our numerical solution of Eq. (4.4) is the most accurate and therefore calculate errors based on this solution. In Fig. 3 we compare results from the different numerical schemes with the solution of Eq. (4.4) (using the solution of Eq. (4.4) as the initial condition). The values $u_l = 0.3323$ and $u_r = 0.1$ are the same as those used in [4]. The figures show the film height around the moving front and a close-up of the peak. The mesh size for the Crank–Nicolson and fully implicit schemes is $h = 0.8$ with a CFL of 0.067. For the explicit methods we can take a larger time-step based on the CFL condition. In fact, we use a CFL of 0.75 for Godunov and upwind and 0.5 for WENO. On Fig. 3a it is difficult to distinguish between the solutions. The distinction is clearer on Fig. 3b. From this close-up it appears that the two implicit methods provide the best approximation to the travelling wave solution. However, these are the solutions on Fig. 3a that produce the large oscillations just downstream of the peak. It is also these two solutions that switch to a lower value for $x < 130$. This strange behaviour can be traced back to oscillations at small time which propagate backwards and act to reduce this left hand limit. Although the oscillations have moved out of the computational domain their effect on the film height remains. Note, the boundary condition at either end is $u_x = 0$. We will discuss this behaviour later in Section 4.2. From Fig. 3b it is clear that the first order Godunov scheme provides the worst result.

Decreasing the space-step allows the implicit schemes to approach the correct left hand limit and also acts to bring all the solutions closer to the travelling wave. This is shown on Fig. 4 when $h = 0.1$. (Note that we fix the CFL numbers for each scheme as in the previous example.) On Fig. 4a only the first order Godunov solution is distinguishable from the rest and this only in the vicinity of the peak. The close-up of Fig. 4b does not capture the first-order Godunov solution. Near the peak it is now the explicit schemes that provide the best solution (with the exception of first-order Godunov). The two implicit schemes bound the explicit and travelling wave solutions.
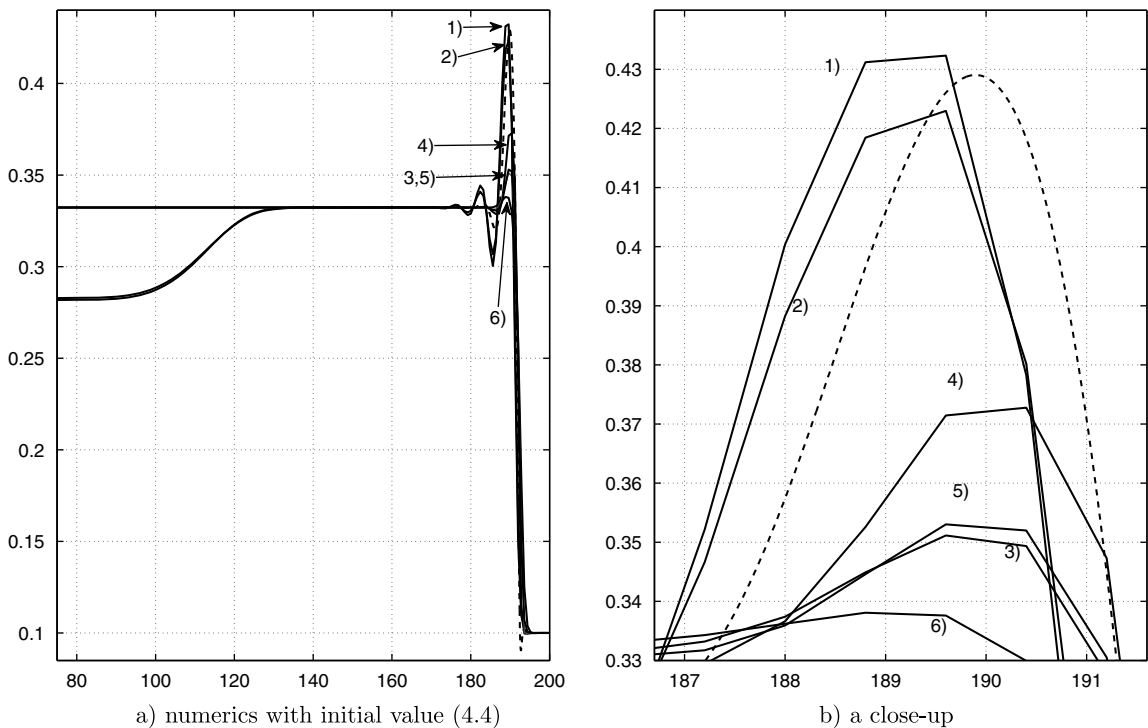

Fig. 3. Comparison of the numerical schemes with the travelling wave solution (4.4) with $u_l = 0.3323$, $u_r = 0.1$ for $h = 0.8$ at time $t = 500$. The curves are (1) Crank–Nicolson, (2) fully implicit, (3) WENO, (4) second order Godunov, (5) adapted upwind and (6) first order Godunov, and the travelling wave (dashed line).
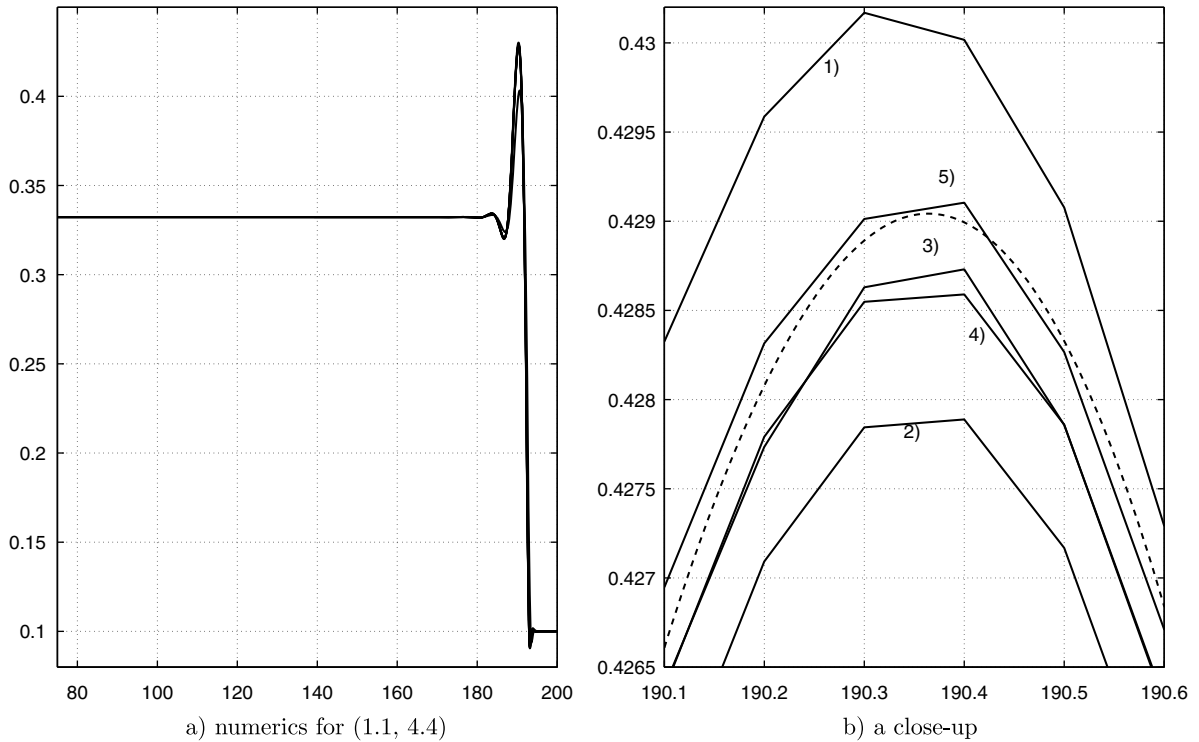
Fig. 4. Comparison of the numerical schemes with the travelling wave solution (4.4) with $u_l = 0.3323$, $u_r = 0.1$ for $h = 0.1$ at time $t = 500$. The curves are (1) Crank–Nicolson, (2) implicit, (3) WENO, (4) second-order Godunov and (5) adapted upwind and the travelling wave (dashed line).

In Table 2 we show the errors and convergence orders of each scheme. Four locations are chosen in distinct parts of the wave and numerical errors at these points are compared. The convergence order is defined in terms of the errors e_h and e_{2h}, corresponding to mesh widths h and $2h$,

$$|e_h| \sim 2^q |e_{2h}|.$$

Therefore, the convergence order is

$$q(h) = \log_2(|e_{2h}|/|e_h|).$$

The orders in the rows corresponding to $h = 0.4$ have been calculated using results for $h = 0.8$ (which are not shown).

The graph of the solution is divided into two parts. The first one is the region smeared by diffusion; points $x = 0$ and 4 are in this region. The other one is the region steepened by convection; corresponding points are $x = 7.2$ and 9.6. Consider the smooth region first. At the point $x = 0$, all the schemes show consistent convergence orders and the smallest size of errors among the four data sets. Convergence orders are about two except the first order Godunov which shows an approximately linear order. The size of the error increases slightly at the point $x = 4$ and the convergence orders show some variations. In particular, WENO and the fully implicit method appears better than the others. Now consider the steep region. At the point $x = 7.2$, the overall error is increased. The convergence order of the implicit schemes is not consistent (in the sense that the order of the error may change sign and does not necessarily increase with decreasing step size). However, the explicit schemes show more reliable behaviour. The first order Godunov scheme still shows a linear convergence order while the other explicit ones show orders around three. The inconsistent behaviour of the implicit schemes may be attributed to the oscillations (which were observed in Figs. 3 and 4). The oscillations are worst where the curvature is highest and obviously they can increase or decrease the maximum value of the peak. Consequently the order of the error may change sign and is most likely to do so at $x = 7.2$ and 9.6 in our

Table 2
Eq. (1.1) is solved up to $t = 30$ with the travelling wave (4.4) as its initial value

Method	Δx	Approximation errors with convergence orders in parentheses			
		$x = 0$	$x = 4$	$x = 7.2$	$x = 9.6$
Crank–Nicolson	0.4	4.3e−4(2.5)	2.0e−3(2.2)	4.9e−4(3.6)	2.4e−3(1.6)
	0.2	1.1e−4(2.0)	5.9e−4(1.9)	5.1e−4(-0.1)	6.0e−4(2.0)
	0.1	3.1e−5(1.8)	2.3e−4(1.4)	6.0e−4(-0.2)	1.2e−3(−1.0)
Fully implicit	0.4	3.7e−4(2.5)	1.0e−3(2.6)	2.9e−3(-5.9)	2.8e−3(-0.7)
	0.2	8.4e−5(2.1)	1.2e−4(3.1)	1.3e−3(1.1)	2.5e−3(0.2)
	0.1	1.9e−5(2.1)	9.5e−6(3.6)	3.7e−4(1.8)	5.3e−4(2.2)
First-order Godunov	0.4	6.8e−4(0.9)	7.4e−3(0.7)	3.7e−2(0.7)	5.6e−2(0.3)
	0.2	3.1e−4(1.1)	4.1e−3(0.8)	2.1e−2(0.8)	3.6e−2(0.6)
	0.1	1.3e−4(1.2)	2.2e−3(0.9)	1.1e−2(0.9)	2.1e−2(0.8)
Second-order Godunov	0.4	1.9e−4(1.7)	1.2e−3(2.1)	7.2e−3(1.8)	1.4e−2(1.4)
	0.2	5.0e−5(1.9)	1.8e−4(2.7)	1.3e−3(2.5)	2.1e−3(2.7)
	0.1	1.2e−5(2.0)	3.5e−5(2.4)	1.3e−4(3.2)	1.6e−4(3.7)
adapted upwind	0.4	3.9e−4(1.6)	3.1e−3(1.6)	1.5e−2(1.6)	3.1e−2(1.2)
	0.2	1.1e−4(1.8)	5.5e−4(2.4)	1.7e−3(3.1)	3.9e−3(3.0)
	0.1	2.8e−5(2.0)	1.1e−4(2.4)	1.5e−4(3.2)	3.1e−4(3.6)
WENO	0.4	2.1e−4(1.8)	1.6e−3(2.2)	1.1e−2(1.7)	2.1e−2(1.2)
	0.2	5.4e−5(2.0)	2.8e−4(2.5)	1.8e−3(2.7)	3.7e−3(2.5)
	0.1	1.3e−5(2.0)	4.0e−5(2.8)	1.2e−4(3.9)	3.6e−4(3.3)
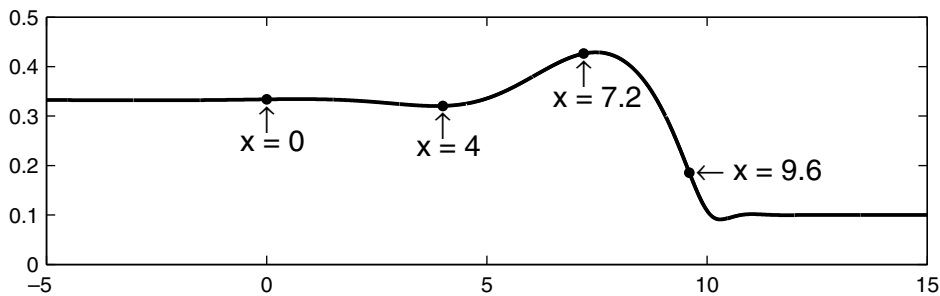
The locations of sample points used in the table.

Numerical approximation errors are given with convergence orders in parentheses.

calculations. With a large step size, $h = 0.8$, the oscillations are at their worst. When $h = 0.4$ the oscillations are much reduced and the errors decrease. Subsequent decreases in the step size result in the peak approaching the travelling wave value in a more sensible manner. The explicit schemes, which do not suffer from the oscillatory behaviour, therefore converge as expected.

The approximation error is largest at the point $x = 9.6$, where the solution has a point of inflexion and therefore the steepest slope among the sample points. The explicit schemes are still consistent here, the implicit ones are not. Considering the small error for the diffusion equation, Table 1, and the observed oscillations in the convection schemes (see Fig. 1) it seems that most of the error comes from convection schemes.

From now on we will use this travelling wave comparison to guide our choice of step size or limiter. We will also neglect the first-order Godunov scheme, which is clearly significantly less accurate than the other schemes. In Fig. 5 we show the effect of changing CFL numbers with $h = 0.1$ on the Crank–Nicolson scheme. The results of Fig. 5a are indistinguishable. From the close-up of the peak, shown on Fig. 5b, we see that values of CFL $\in [0.033, 0.042]$ give a good approximation around the peak for this choice of h. Using similar comparisons we find the MC limiter and $\alpha = 1.35$ provide the best results for Godunov and upwind schemes respectively. The WENO method appears to be robust with respect to changes in the CFL number, with the solutions showing little variation for a CFL $\in [0.4, 0.6]$. We will discuss these choices in Section 4.3.
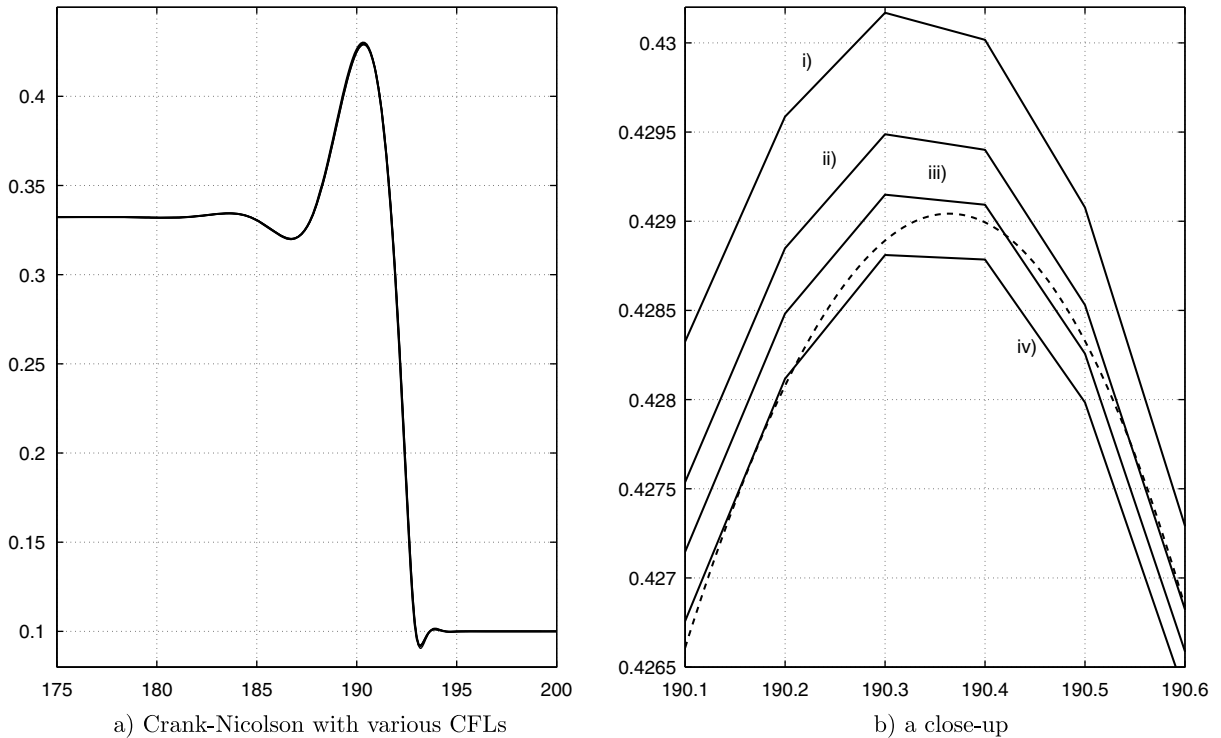
Fig. 5. The effect of changing CFL numbers, for fixed $h = 0.1$, on the Crank–Nicolson solution with discontinuous initial value at time $t = 500$. The curves are (i) CFL $= 0.0667$, (ii) 0.05, (ii) 0.0417 and (v) 0.0333.

4.2. Effect of the moving grid substitution

We now consider the effect of adding the term $-su_x$ to the travelling wave of the previous section. If we take continuous initial data, such as that given in [4] then all solutions agree well, for sufficiently small space and time-step. However, when we start with discontinuous initial data, switching from u_l to u_r at $x = 0$ significant differences arise. Four sets of results for discontinuous initial data are shown on Fig. 6. The first two, Fig. 6a and b, show solutions including the $-su_x$ term. The Crank–Nicolson result is shown as a dashed line, the remaining solutions coincide, even to the level of the close-up of Fig. 6b, and are shown as the solid line. The final figures, Fig. 6c and d, show results without the $-su_x$ term. The travelling wave and explicit schemes all coincide. As in Fig. 3a the two implicit schemes, shown as dashed lines, tend to a lower left hand limit, although in the current situation the correct limit is never attained. Again this strange behaviour is a result of the initial oscillations caused by the discontinuity. This oscillation travels backwards and leads to the left hand limit slightly decreasing. The explicit schemes that avoid the oscillation do not suffer from this problem. In this case, the maximum wave height predicted by Crank–Nicolson and implicit schemes is also slightly lower and therefore slower than the explicit waves. If we begin with continuous data the results are all very similar to the explicit results for discontinuous data.

The change in behaviour between the figures is a result of the numerical scheme applied to the $-su_x$ term. The explicit schemes can all handle (and reduce) the oscillations that result from the application of the implicit diffusion term to discontinuous data. On the other hand the Crank–Nicolson and implicit terms propagate the oscillations. For consistency and to prevent the numerical treatment of the $-su_x$ term from affecting the results (somewhat erroneously as it now appears) we apply the central method to this term for all schemes. Like the tested explicit schemes, this method acts to reduce the oscillations and so improves the results for the implicit methods. Note, if we apply one of the other explicit schemes to this term it would also remove problem. If we use an implicit method to deal with the term then the problem remains.
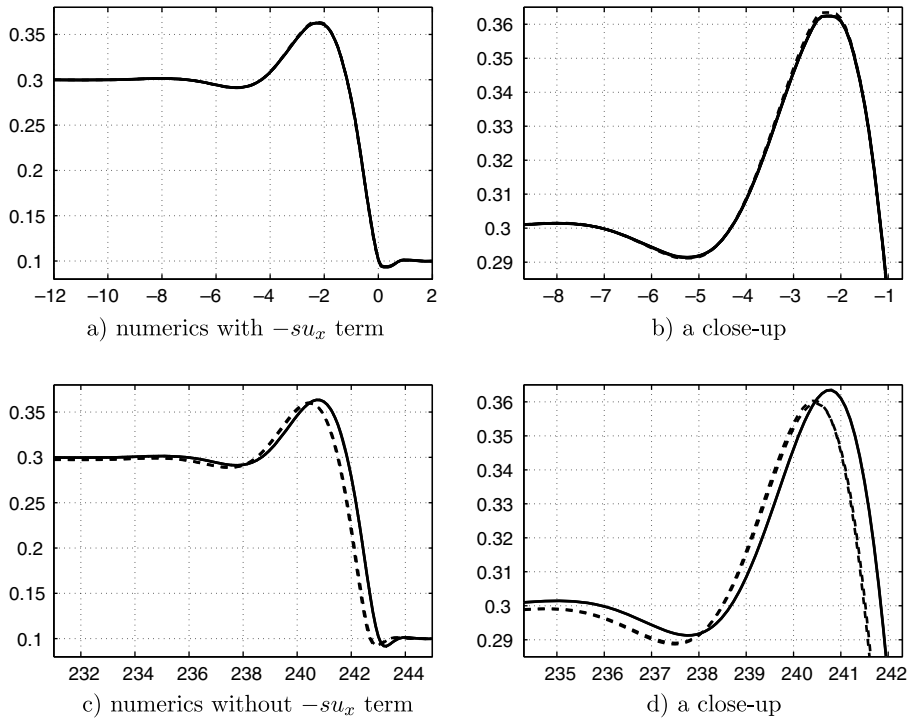
Fig. 6. Travelling waves with discontinuous initial data at $t = 900$, $h = 0.1$. Implicit schemes are shown as dashed lines and the exact and explicit ones as solid lines.

This indicates a good reason to use the explicit schemes, which show consistent results regardless of the initial data. Further, the smaller time step of the implicit schemes means that they take more than twice the time required by the explicit schemes to produce a result.

4.3. Stable travelling waves?

Bertozzi et al. [4] point out that for a range of far field heights, the system (1.1) and (1.2) can support multiple shock profiles, but only two are stable. The first case they present uses a hyperbolic tangent initial profile with $u_l = 0.3323$, $u_r = 0.1$. The results are identical to those shown in our first example, in Section 4.1. The second stable wave involves an initial condition with a bump of width 10,

$$u(x) = \begin{cases} \frac{0.6-u_l}{2} \tanh(x + 5) + \frac{0.6+u_l}{2} & \text{for } x < 0 \\ -\frac{0.6-u_r}{2} \tanh(x - 5) + \frac{0.6+u_r}{2} & \text{for } x > 0, \end{cases} \quad (4.5)$$

where $u_l = 0.3323$ and $u_r = 0.1$. Note, we have shifted the origin from that given in [4], since the governing equation is autonomous this will not affect the results. However, when the bump width is increased to 20, at large times the bump appears to spread out and so is classified as unstable.

In Fig. 7 we present results for the initial profile of Eq. (4.5) at $t = 10^4$. In this case we solve the governing equation with a moving axis, given by Eq. (4.1). The Godunov and WENO results are hard to distinguish, so we have labelled them as a single curve. For the Crank–Nicolson and implicit schemes we still take CFL= 0.0667. The CFL numbers for explicit schemes are 0.5 for WENO and 0.75 for Godunov and upwind. All curves show that the initial hump changes to an undercompressive wave on the right and a compressive wave on the left. The bump width remains relatively constant for each scheme. This wave therefore appears stable.

Switching the initial condition, by replacing the 5 in Eq. (4.5) with a 10 (and so a bump of width 20), leads to the results for $t = 10^5$ shown in Fig. 8. The fully implicit scheme, which appears reasonable at $t = 10^4$ has
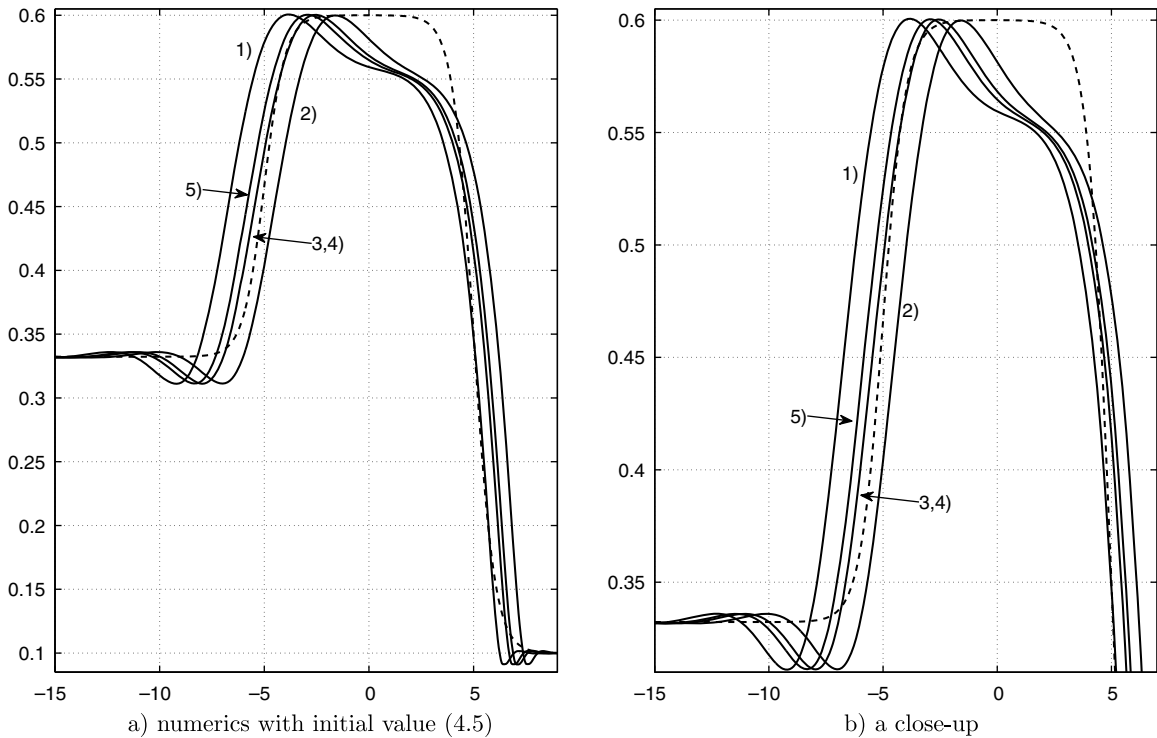
Fig. 7. The curves are (1) Crank–Nicolson, (2) fully implicit, (3) WENO, (4) second order Godunov and (5) adapted upwind and the initial condition (dashed line). Here, $h = 0.05$.

moved out of the computational domain at 10^5 and so is not shown. In Fig. 8a we see the effect of changing CFL numbers on the evolution of the travelling wave using the Crank–Nicolson scheme. When CFL = 0.0667 the wave speed is less than that predicted by Rankine–Hugoniot. Further, the back and front ends of the wave move at a different speed resulting in the wave spreading out. This gives the appearance that the wave is unstable. Decreasing the CFL number does not necessarily fix the problem. With CFL = 0.0333 the wave moves slightly too fast and also acts to reduce the width of the bump. In Section 4.1 we mentioned choosing a CFL number to give the least error compared to the travelling wave example of that section and suggested choosing CFL $\in [0.033, 0.042]$. From Fig. 8a we see when CFL = 0.0417 the downstream edge of the wave matches the initial data. The upstream edge is slightly out, but of all cases this shows the least change in bump width. Similarly, with Godunov we found the MC limiter provided the best results and $\alpha \sim 1.35$ for upwind. These are shown in Fig. 8b and c respectively. WENO appeared relatively stable to changes in the CFL number. This is confirmed in Fig. 8d.

The results of Fig. 8 indicate that this form of travelling wave is not unstable. It is merely the choice of numerical scheme and step sizes that lead to the bump spreading. In particular we note that WENO shows very little spread for a range of CFL numbers. The Godunov scheme appears sensitive to the choice of limiter. The SB limiter allows the bump to spread considerably, whereas MC and VL limiters maintain the initial width, with MC perhaps moving at the better speed. The upwind scheme maintains the correct width when $\alpha \approx 1.25$ (slightly lower than the value 1.35 predicted earlier).

4.4. Double shock travelling wave

In our final example we examine the evolution of a double shock wave. This corresponds to Case 3 in [4]. In all cases we use the step sizes or limiters that have so far provided the best results. So far in this section, we have chosen examples where $u_l < 1/3$, which is where the flux has a point of inflexion. The following example
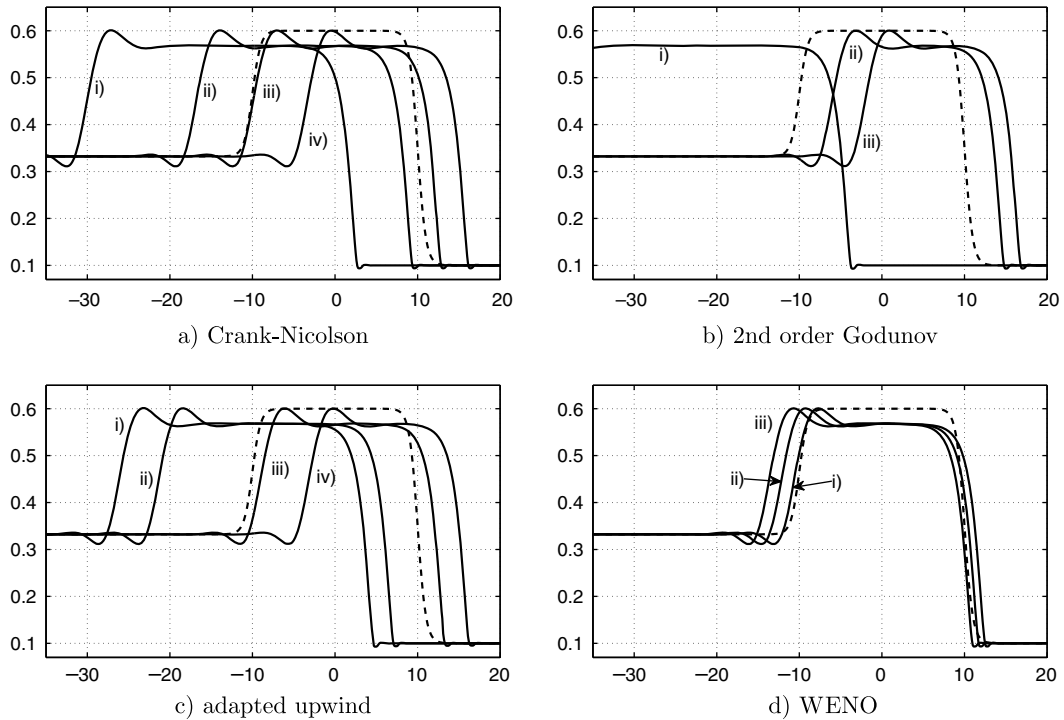
Fig. 8. Results at $t = 10^5$, with $h = 0.1$. The initial condition is a dashed line and (a) with CFL=(i) 0.0667, (ii) 0.05, (iii) 0.0417, (iv) 0.0333, (b) with (i) SB, (ii) MC, (iii) VL, (c) with (i) $\alpha = 1.95$, (ii) 1.5, (iii) 1.25, (iv) 1.2 and (d) with CFL=(i) 0.4, (ii) 0.5, (iii) 0.6.
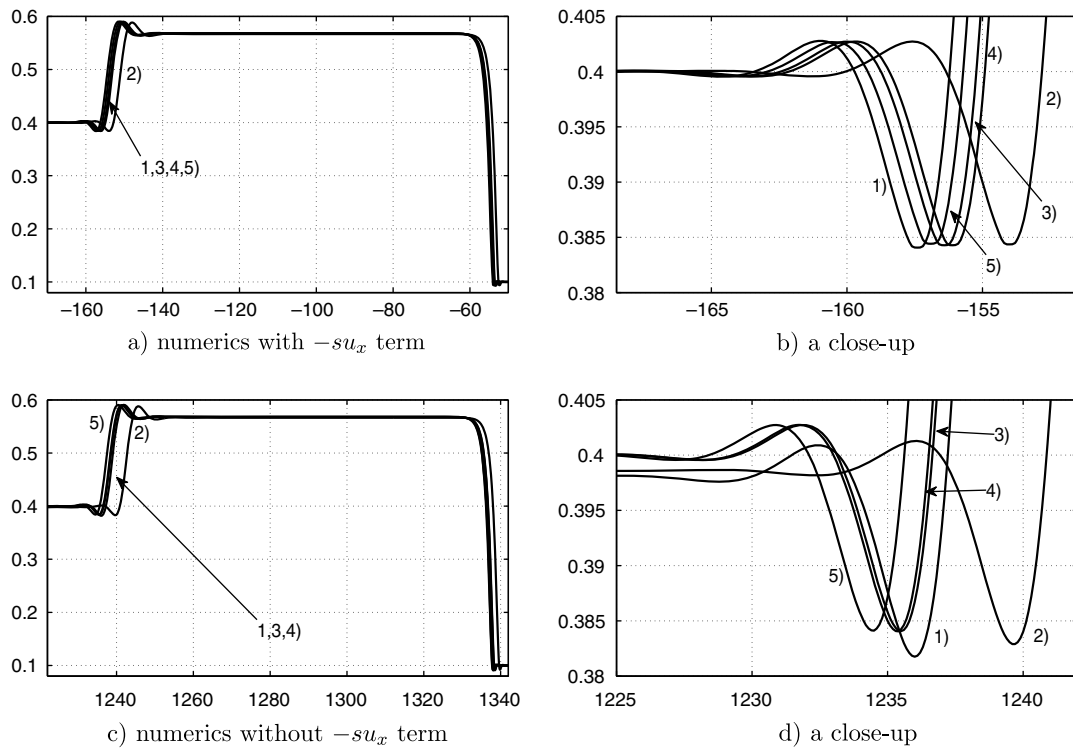

Fig. 9. Double shock with discontinuous initial condition at time=4800 $h = 0.1$, CFL = 0.0667 for (1) Crank–Nicolson and (2) fully implicit, CFL = 0.5 for (3) WENO, and CFL = 0.75 for (4) second order Godunov and (5) adapted upwind.

shows the large effect that a small change in u_l can have. With continuous initial data all the schemes provide similar results. In Fig. 9 we present solutions for the discontinuous initial data, $u = 0.4$ for $x < 0$, $u = 0.1$ for $x \geqslant 0$. Fig. 9a and b show the solution near the travelling hump, including the $-su_x$ term and also a close up of the downstream edge of the hump. In the close-up of Fig. 9b we can see that the implicit schemes bound the explicit ones. Without the $-su_x$ term, as in previous examples we see that the implicit schemes tend to a lower left hand limit. The implicit solution has also travelled further away from the other results.

5. Conclusion

We have presented a comparison of numerical schemes applied to a fourth-order thin film equation, with particular examples taken from the work of Bertozzi et al. [4]. The results presented allow us to make a number of conclusions and recommendations regarding the numerical approximation of such schemes.

Firstly, we noted that applying a fractional step-splitting method using an explicit scheme for the convection term and an implicit one for the fourth-order diffusion term provides much more stable results than when treating the whole equation using an implicit method. If diffusion is neglected altogether, then all the methods considered dealt well with sufficiently continuous initial data. With discontinuous (on the scale of the space-step) initial data the implicit schemes all led to oscillations, while the explicit methods coped well. Of the explicit schemes WENO produced the least accurate result for the second discontinuous example.

When the fourth-order diffusion term is included it is clear that implicit methods should be applied to speed up calculations. We examined the effect of applying implicit schemes to the whole equation or combining an implicit diffusion scheme with an explicit convection one. The schemes that include an explicit step turned out to allow much larger time-steps. Further, the explicit results showed smaller errors and higher convergence order when compared to a standard travelling wave solution. Hence we conclude that the 'explicit' convection schemes are more computationally efficient and more accurate than the implicit ones.

When available the travelling wave solution can be used to determine appropriate values for time and space steps, limiters or the value of the CFL number. We carried this out in Section 4.1. For each method, except for upwind where we were slightly out, our choice led to the best results in the example of Section 4.3. With the exception of WENO, the comparison in Section 4.3 highlighted the sensitivity of the methods to the limiter or time-step. WENO provided consistent and accurate results.

The use of discontinuous initial data led to surprising results. With the implicit schemes in particular, an oscillation at early time resulted in the large time solution tending to an incorrect downstream limit. Possibly this could be fixed by specifying the limit value as a boundary condition, rather than using a zero derivative condition. However, it does highlight a possible problem with the implementation of the method. The explicit schemes all handled the discontinuity with no apparent problem. Note, as in the first example of Section 4.1 discontinuous can simply mean that changes occur over a smaller length-scale than the space-step. When the convective term $-su_x$ was included the problem with the implicit schemes was removed. This was a result of applying the central method to this term which gave the scheme a similar form to our other explicit schemes.

To summarize, from our calculations it appears that for the best accuracy and efficiency fourth-order diffusion equations with a convective term should be tackled using an explicit method on the convection term coupled to an implicit diffusion term by fractional step-splitting. The choice of explicit methods may be guided by a travelling wave solution. Our examples indicate that for this type of problem WENO is the most robust of the three methods investigated.

References

[1] N. Balmforth, S. Ghadge, T.G. Myers, Surface tension driven fingering of a viscoplastic film, J. Non-Newtonian Fluid Mech. 142 (2007) 143–149.

[2] A.L. Bertozzi, M.P. Brenner, T.F. Dupont, L.P. Kadanoff, Singularities and similarities in interface flows, Trends and Perspectives in Applied Mathematics, Springer-Verlag, New York, 1994, pp. 155–208.

[3] A.L. Bertozzi, A. Munch, X. Fanton, A.M. Cazabat, Contact line stability and undercompressive shocks in driven thin film flow, Phys. Rev. Lett. 81 (23) (1998) 5169–5172.

[4] A.L. Bertozzi, A. Munch, M. Shearer, Undercompressive shocks in thin film flows, Physica D 134 (1999) 431–464.

[5] J.B. Greer, A.L. Bertozzi, G. Sapiro, Fourth order partial differential equations on general geometries, J. Comput. Phys. 216 (1) (2006) 216–246.

[6] S.K. Godunov, Mat. Sbornik 47 (1959) 271.

[7] Y. Ha, C.L. Gardner, A. Gelb, C.-W. Shu, Numerical simulation of high mach number astrophysical jets with radiative cooling, J. Sci. Comput. 24 (2005) 29–44.

[8] Y. Ha, Y.-J. Kim, Explicit solutions to a convection-reaction equation and defects of numerical schemes, J. Comput. Phys. 220 (1) (2006) 511–531.

[9] G.-S. Jiang, D. Levy, C.-T. Lin, S. Osher, E. Tadmor, High-resolution non-oscillatory central schemes with non-staggered grids for hyperbolic conservation laws, SIAM J. Numer. Anal. 35 (1998) 2147–2168.

[10] G.-S. Jiang, C.-W. Shu, Efficient implementation of weighted ENO schemes, J. Comput. Phys. 126 (1) (1996) 202–228.

[11] D.E. Kataoka, S.M. Troian, A theoretical study of instabilities at the advancing front of thermally driven coating films, J. Colloid Interf. Sci. 192 (2) (1997) 350–362.

[12] J.S. Kim, Adaptive mesh refinement for g1thin-film equations, J. Korean Phys. Soc. 49 (5) (2006) 1903–1907.

[13] Y.-J. Kim, Piecewise self-similar solutions and a numerical scheme for scalar conservation laws, SIAM J. Numer. Anal. 40 (6) (2002) 2105–2132.

[14] Y.-J. Kim, Y. Ha, Fundamental solutions of a conservation law without convexity, <http://amath.kaist.ac.kr/~ykim/preprints/14.pdf>.

[15] Y.-J. Kim, Y. Lee, Structure of fundamental solutions of a conservation law without convexity, <http://amath.kaist.ac.kr/~ykim/preprints/17.pdf>.

[16] A. Kurganov, S. Noelle, G. Petrova, Semi-discrete central-upwind schemes for hyperbolic conservation laws and Hamilton–Jacobi equations, SIAM J. Sci. Comput. 23 (2001) 707–740.

[17] A. Kurganov, E. Tadmor, New high-resolution central schemes for nonlinear conservation laws and convection–diffusion equations, J. Comput. Phys. 160 (2000) 214–282.

[18] R.J. LeVeque, Numerical methods for conservation laws, Lectures in Mathematics ETH Zürich, Birkhäuser Verlag, Basel, 1990.

[19] R.J. LeVeque, High-resolution conservative algorithms for advection in incompressible flow, SIAM J. Numer. Anal. 33 (1996) 627–665.

[20] X.-D. Liu, S. Osher, T. Chan, Weighted essentially non-oscillatory schemes, J. Comput. Phys. 115 (1994) 200–212.

[21] T.G. Myers, Thin films with high surface tension, SIAM Rev. 40 (3) (1998) 441–462.

[22] T.G. Myers, J.P.F. Charpin, C.P. Thompson, Slowly accreting ice due to supercooled water impacting on a cold surface, Phys. Fluids 14 (1) (2002) 240–256.

[23] T.G. Myers, J.P.F. Charpin, S.J. Chapman, The flow and solidification of a thin fluid film on an arbitrary three-dimensional surface, Phys. Fluids 14 (8) (2002) 2788–2803.

[24] H. Nessyahu, E. Tadmor, Non-oscillatory central differencing for hyperbolic conservation laws, J. Comput. Phys. 87 (2) (1990) 408–463.

[25] A. Oron, S.H. Davis, S.G. Bankoff, Long-scale evolution of thin liquid films, Rev. Modern Phys. 69 (3) (1997) 931–980.

[26] V.V. Rusanov, The calculation of the interaction of non-stationary shock waves with barriers, Ž. Vyčisl. Mat. i Mat. Fiz. 1 (1961) 267–279.

[27] R.D. Russell, J.F. Williams, X. Xu, MOVCOL4: a moving mesh code for fourth-order time-dependent partial differential equations, SIAM J. Sci. Comput. 29 (1) (2007) 197–220.

[28] C.-W. Shu, S. Osher, Efficient implementation of essentially non-oscillatory shock capturing schemes, J. Comput. Phys. 77 (1988) 439–471.

[29] C.-W. Shu, S. Osher, Efficient implementation of essentially non-oscillatory shock capturing schemes, II, J. Comput. Phys. 83 (1989) 32–78.

[30] C.-W. Shu, S. Osher, Essentially non-oscillatory and weighted essentially non-oscillatory schemes for hyperbolic conservation laws, in: B. Cockburn, C. Johnson, C.-W. Shu, E. Tadmor (Eds.), Advanced numerical approximation of nonlinear hyperbolic equations, in: A. Quarteroni (Ed.), Lecture Notes in Mathematics, vol. 1697, Springer, 1998, p. 325.

[31] E.F. Toro, Riemann Solvers and Numerical Methods for Fluid Dynamics: A Practical Introduction, Springer, 1999.

[32] B. van Leer, MUSCL, A new approach to numerical gas dynamics, in: Computing in Plasma Physics and Astrophysics, Max-Planck-Institut für Plasma Physik, Garchung, Germany, April 1976.

[33] D. Vaynblat, J.R. Lister, T.P. Witelski, Rupture of thin viscous films by van der Waals forces: evolution and self-similarity, Phys. Fluids 13 (5) (2001) 1130–1140.